

Supplementary Materials for

Cryo-EM structure of the activated RET signaling complex reveals the importance of its cysteine-rich domain

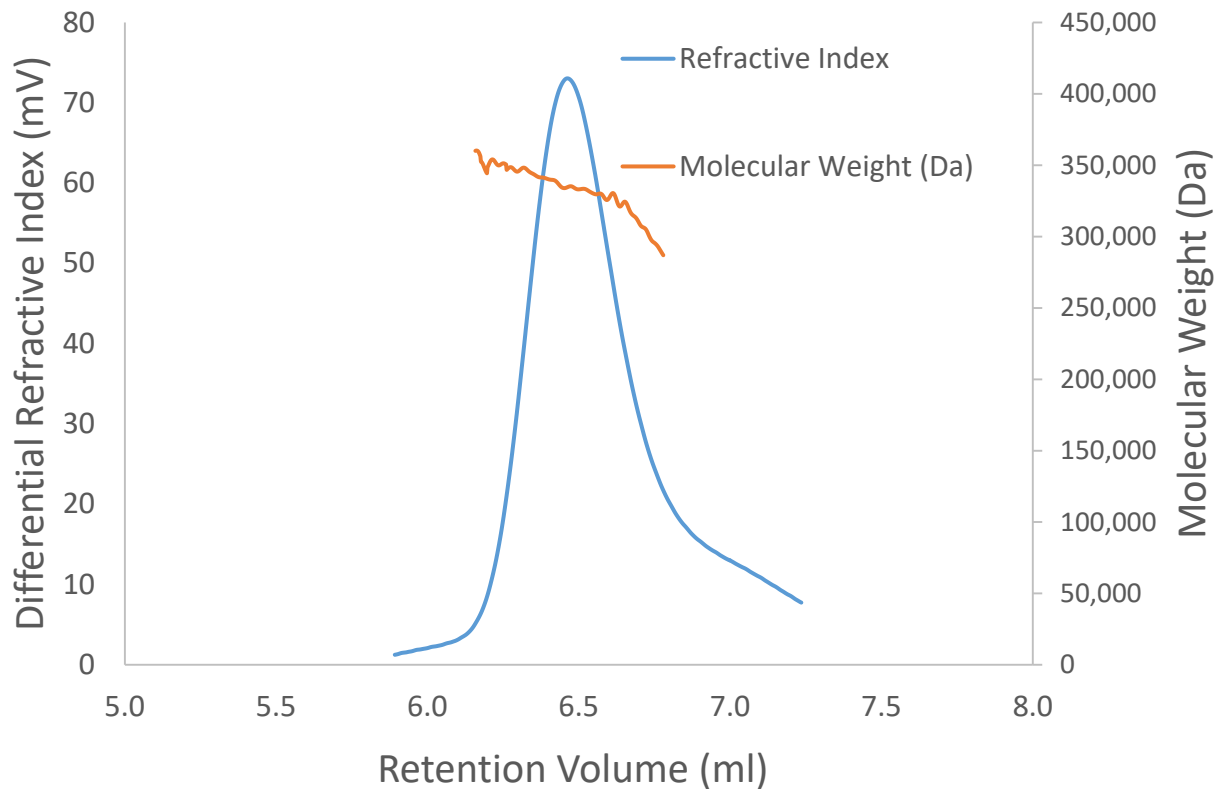
Janna M. Bigalke, Shintaro Aibara, Robert Roth, Göran Dahl, Euan Gordon,
Sarah Dorbéus, A. Amunts*, Jenny Sandmark*

*Corresponding author. Email: amunts@scilifelab.se (A.A.); jenny.sandmark@astrazeneca.com (J.S.)

Published 31 July 2019, *Sci. Adv.* **5**, eaau4202 (2019)
DOI: 10.1126/sciadv.aau4202

This PDF file includes:

- Fig. S1. SEC-MALS of the wild-type extracellular signaling complex.
- Fig. S2. Cryo-EM data processing.
- Fig. S3. RET^{ECD} glycosylations.
- Fig. S4. SEC of the heterohexameric complex and its components.
- Fig. S5. Biophysical analysis of complex formation.
- Fig. S6. Related GFL-GFR α crystal structures display varying angles of GFR α positions in relation to the GFL center.
- Table S1. Cryo-EM data collection, refinement, and validation statistics.



Protein/Complex	MALS MW (kDa)	Calculated Protein MW (kDa)	Peptide Fraction (kDa)	Glycosylation MW (kDa)
GFR α 2	65 \pm 3	48	49	18
RET	103 \pm 7	69	73	30
RET-GFR α 2-NRTN	328 \pm 9	255	247	74

Fig. S1. SEC-MALS of the wild-type extracellular signaling complex. The molecular weight of the hexameric complex and its separate components was determined by SEC-MALS. The wildtype heterohexamer eluted as a single symmetric peak with a molecular weight of 330 kDa (top panel). The peptide fraction of the complex was shown to have a molecular weight of 247 kDa which agrees well with the expected value, confirming that the heterohexamer is heavily glycosylated (table). Furthermore, GFR α 2 and RET when analysed separately were also shown to be glycosylated. The signal from NRTN was obscured by the buffer agents that co-elute and could therefore not be detected. The average of three experiments is reported.

MW – Molecular weight

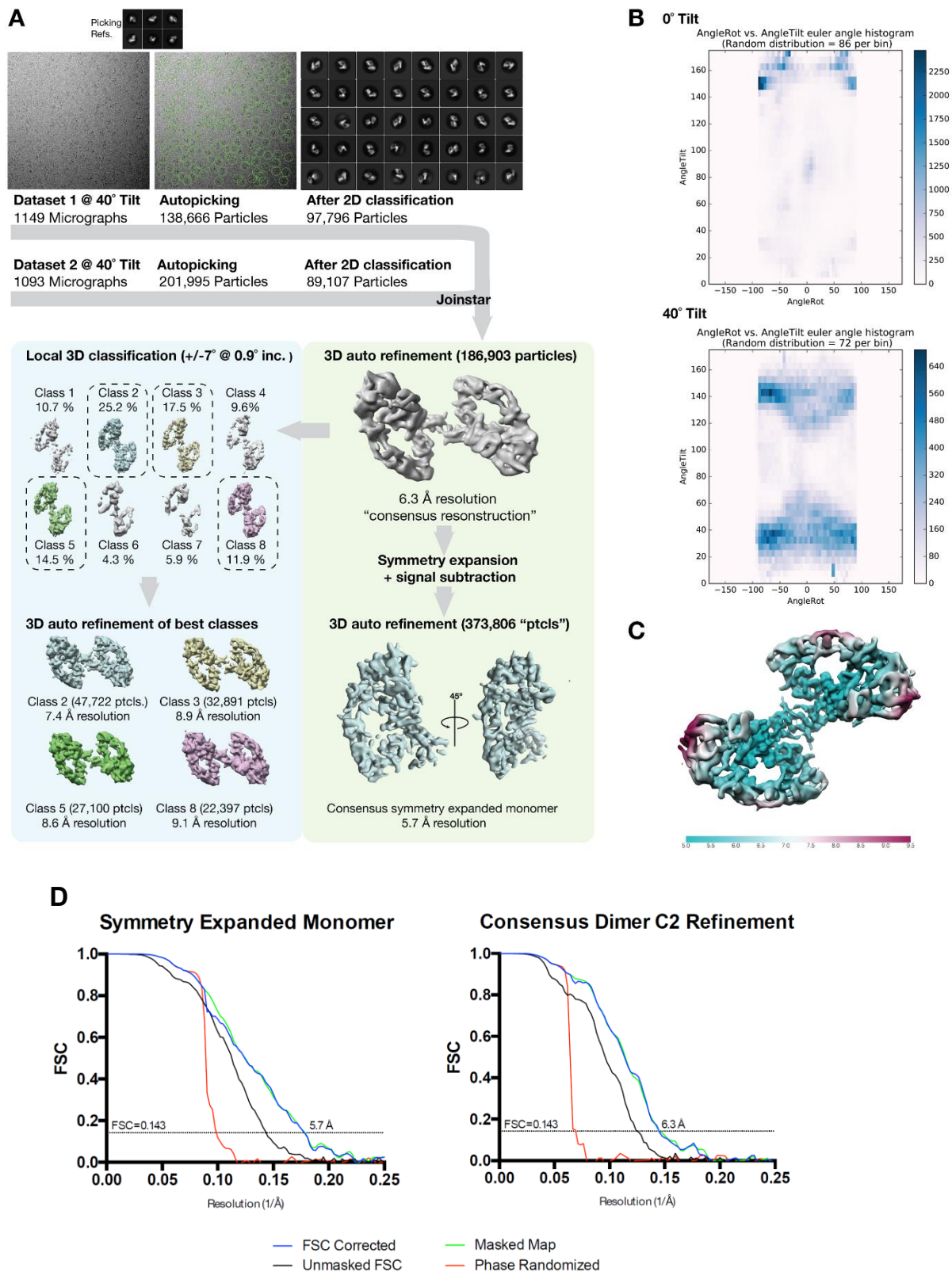


Fig. S2. Cryo-EM data processing. **A.** Flow-chart of data processing. **B.** Histogram plot comparing the Euler angular distributions between 3D reconstructions calculated from a dataset with no tilt (top) and 40 degrees tilt (bottom) **C.** Local resolution estimates for the 6.3 Å consensus refined map. **D.** Fourier shell correlation plot for half-maps. The overall resolution is estimated to be 5.7 Å based on the FSC = 0.143 cut-off criterion for the symmetry expanded monomer. Without symmetry expansion the “consensus reconstruction” has an estimated resolution of 6.3 Å.

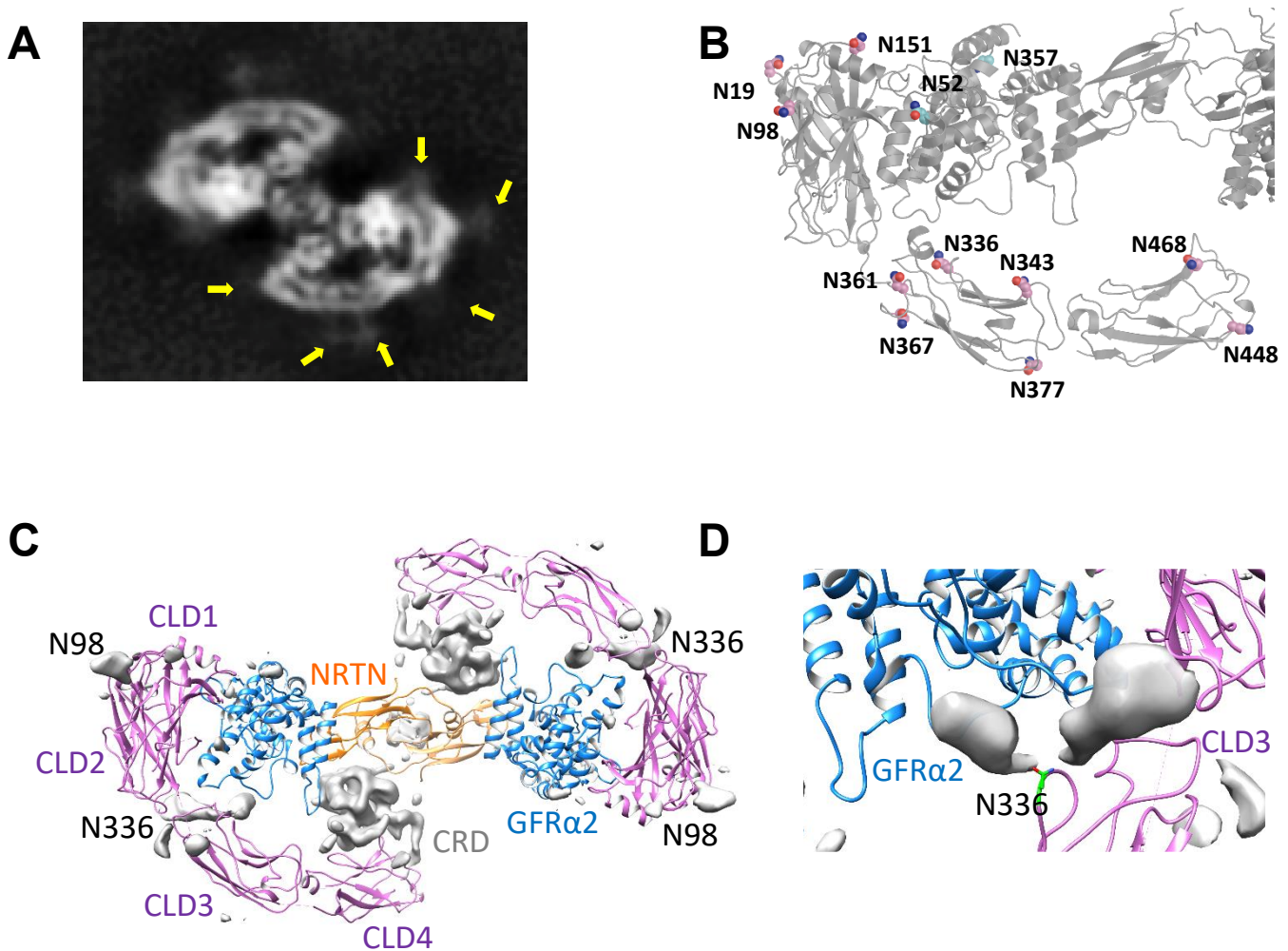
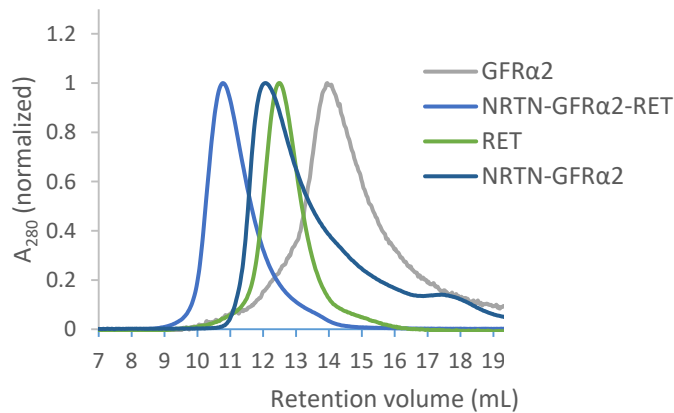


Fig. S3. RET^{ECD} glycosylations. **A.** Protrusions (yellow arrows) were visible in the 2D class averages and were identified to be six (out of 11) of the glycans linked to RET^{ECD}. **B.** 10 of 11 N-linked glycosylation sites in RET^{ECD} (pink) and 2 of 3 in GFR α 2 (light blue) are shown as spheres. Additional glycosylation sites are located on unmodelled parts of the structure. Most of the glycans are solvent exposed, however at least one, connected to N336, is pointing towards GFR α 2. **C.** Difference density maps (grey) showing the glycans linked to N336 and N98 (labelled) in RET^{CLD3} and the unmodelled RET^{CRD}. The modelled parts of the cryo-EM structure are shown as cartoon, NRTN in orange, GFR α 2 in blue and RET^{CLD1-4} in pink. **D.** Close up view of the difference density for the glycan linked to N336 (green, stick representation) in RET^{CLD3} (pink, cartoon). The difference density shows that a branched sugar chain is pointing towards GFR α 2 (blue, cartoon). The panel is rotated compared to the view in C.

A

SEC (Superdex200 10/300)

**B**

SEC (Superdex200 10/300)

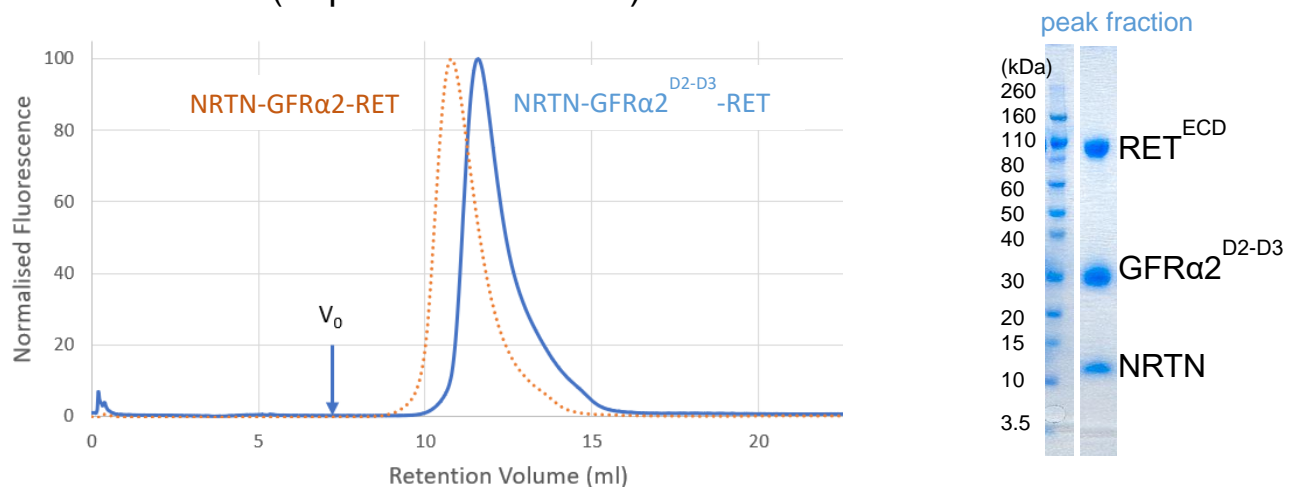


Fig. S4. SEC of the heterohexameric complex and its components. **A.** Elution profiles of wildtype proteins RET^{ECD} and $\text{GFR}\alpha 2$, the bipartite complex $\text{NRTN-GFR}\alpha 2$ and the heterohexamer $\text{NRTN-GFR}\alpha 2\text{-RET}^{\text{ECD}}$. $\text{NRTN-GFR}\alpha 2$ and RET^{ECD} elute from the Superdex 200 column at similar retention volumes. The heterohexameric complex elutes much earlier. Both RET^{ECD} and $\text{GFR}\alpha 2$ appear larger than their actual size (68 and 47 kDa respectively) due to glycosylation as shown by SEC-MALS (Fig. S1). **B.** Size exclusion chromatography of the signalling complex with a truncated $\text{GFR}\alpha 2$ protein missing domain 1 and the flexible C-terminus ($\text{GFR}\alpha 2^{\text{D2-D3}}$, blue trace). The complex elutes as a single monodisperse peak from the Superdex 200 column, suggesting that the heterohexamer complex formation is unaffected by the removal of $\text{GFR}\alpha 2$ domain 1 and the C-terminus. The peak fraction was analysed by SDS-PAGE and is shown on the right. The size exclusion chromatogram for the extracellular signalling complex with full-length $\text{GFR}\alpha 2$ is superimposed for comparison (orange dotted trace).

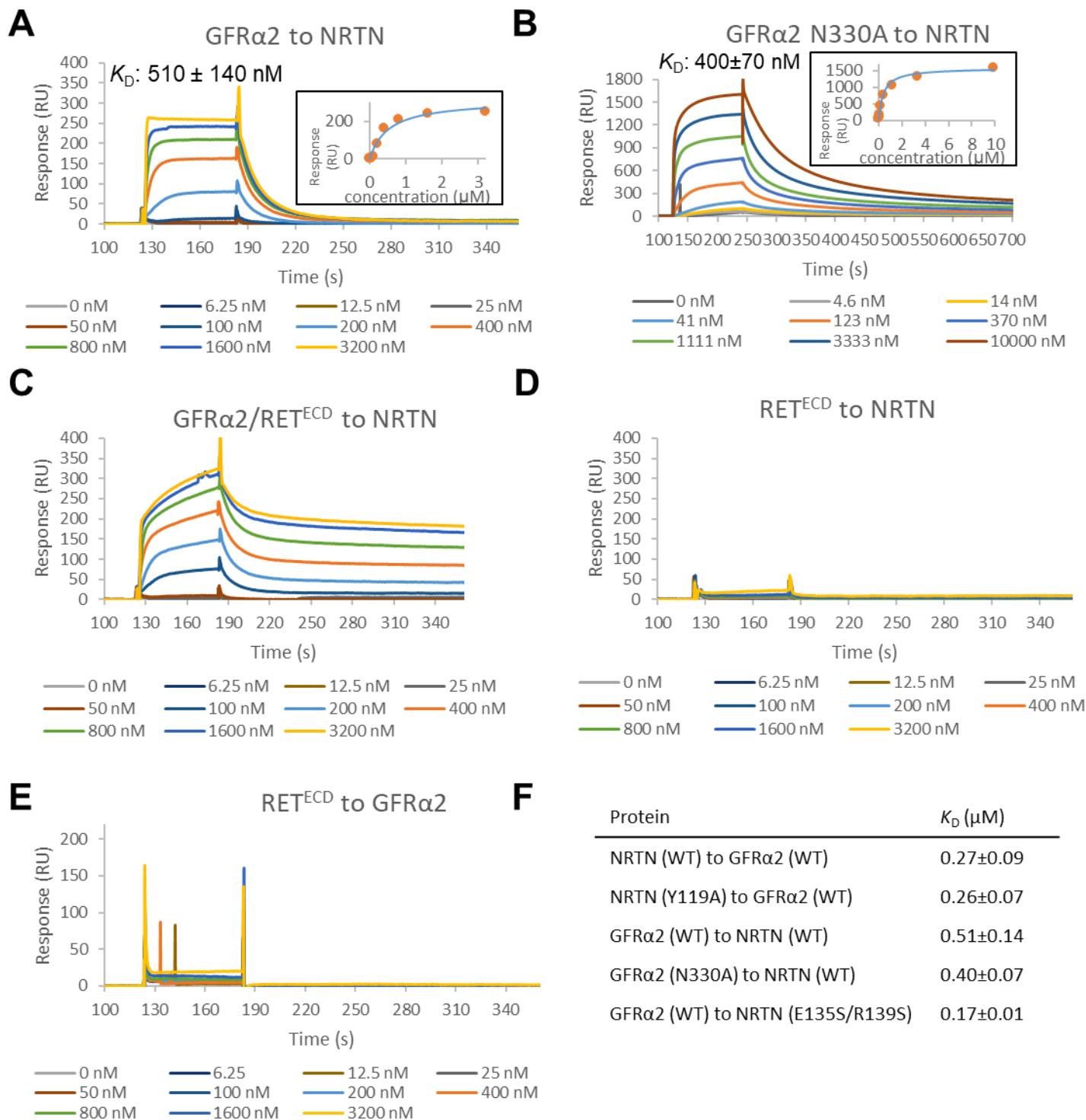


Fig. S5. Biophysical analysis of complex formation. SPR was used to analyse the subunit interactions within the complex. **A-B.** GFR α 2-binding to immobilized NRTN revealed a similar K_D (510 ± 140 nM) as GFR α 2 N330A to NRTN (400 ± 140 nM). Insets show equilibrium responses plotted against concentration, which were used to fit the data. **C.** When NRTN is immobilized and the other two proteins of the complex (GFR α 2/RET^{ECD}) are injected simultaneously, a binding signal stronger than GFR α 2 alone can be observed (A). Furthermore, an apparent slower dissociation can be observed. The equilibrium dissociation constants cannot be determined by this method, because the binding response never reaches equilibrium. **D.** RET^{ECD} does not bind to NRTN alone. **E.** RET^{ECD} does not bind to GFR α 2 alone. **F.** K_D values for the NRTN-GFR α 2 interaction, with either NRTN or GFR α 2 immobilized on the sensor chip. WT – wildtype.

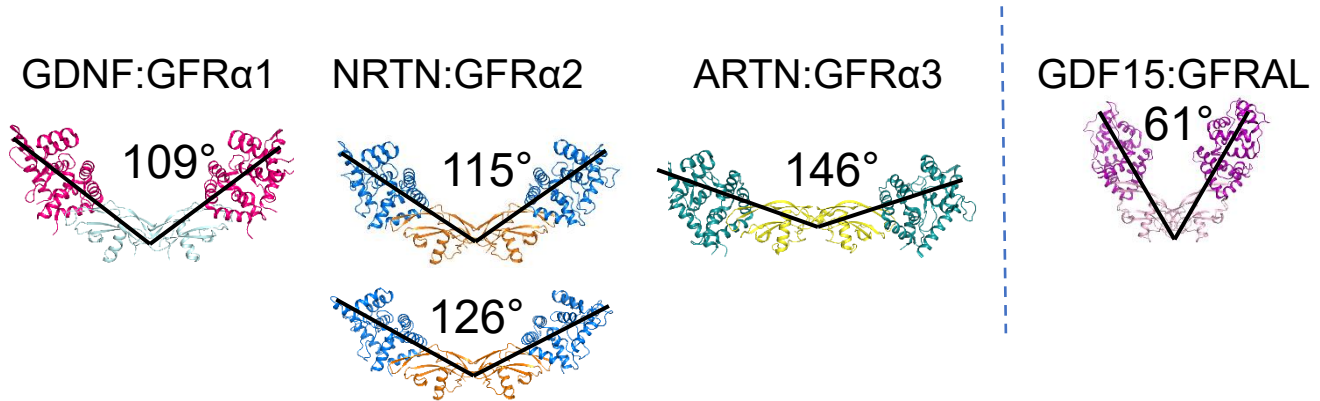


Fig. S6. Related GFL-GFR α crystal structures display varying angles of GFR α positions in relation to the GFL center. All crystal structures that have been solved so far display conformational differences, similar to the differences seen in our cryo-EM sample (Fig. 5).

Table S1. Cryo-EM data collection, refinement, and validation statistics.

Data Collection	
Particles	186,903 (373,806)
Pixel size (Å)	1.05
Defocus range (µm)	0.4-4.5
Voltage (kV)	300
Electron dose (e ⁻ Å ⁻²)	38
Model Composition	
Non-hydrogen atoms	13470
Protein residues	1694
Refinement	
Resolution (Å)	5.7 – 6.3
Map sharpening B-factor (Å ²)	Various
Average B Factor (Å ²)	220
Rmsd Deviations	
Bonds (Å)	0.01
Angles (°)	1.1
Validation	
Molprobrity Score	1.48 (96th Percentile)
Clashscore, all atoms	3.92 (96th Percentile)
Good Rotamers (%)	100
Cβ-deviations	0
Ramachandran Plot	
Favored (%)	95.72
Outliers (%)	4.28